Detection of Crystalline and Fine-grained Calcic Plagioclases on Vesta

E. Palomba[1] , E. D'Aversa[1] , T. M. Sato[2,3], A. Longobardo[1,4], F. Dirri[1], S. Aoki[5,6], G. Orton[7], G. Sindoni[1], F. Oliva[1] ,
G. Carrozzo[1], and Y. Kasaba[8]

[1] INAF-IAPS, via del Fosso del Cavaliere 100, I-00133 Rome, Italy; ernesto.palomba@inaf.it
[2] ISAS-JAXA, Sagamihara, Kanagawa 252-5210, Japan
[3] Hokkaido Information University, Ebetsu, Hokkaido 069-8585, Japan
[4] DIST-Università Parthenope, Centro Direzionale Isola C4, 80143, Naples, Italy
[5] Planetary Aeronomy, Royal Belgian Institute for Space Aeronomy, 3 av. Circulaire, B-1180 Brussels, Belgium
[6] Fonds National de la Recherche Scientifique, rue d'Egmont 5, B-1000 Brussels, Belgium
[7] NASA/Jet Propulsion Laboratory, California Institute of Technology, 4800 Oak Grove Drive, Pasadena, CA 91109, USA
[8] Planetary Plasma and Atmospheric Research Center, Graduate School of Science, Tohoku University, Sendai, Miyagi 980-8578, Japan

Abstract

Plagioclase feldspars are among the most prevalent minerals in the solar system, and are present in many chondritic and achondritic meteorite families. Nevertheless, spectral features of plagioclases have never been unambiguously and directly observed in remote observations of asteroids. We report here the detection of an absorption band at 12.2 μm on Vesta spectra provided by ground-based spectral observations at the Subaru Telescope. This signature represents the first direct evidence of a widespread presence of crystalline Ca-rich plagioclase on Vesta and reveals that its regolith is comminuted to a very fine grain size, smaller than a few tens of microns, indicating that the mechanical brecciation process has been very effective. The crystalline nature of plagioclase strongly suggests that impacts alone cannot be the sole mechanism for regolith formation on Vesta and a milder process, such as thermal fatigue, should be invoked as an important and concomitant process Thermal fatigue should be considered a very effective process in regolith production and rejuvenation not only for near-Earth asteroids but even for large asteroids located in the main belt.

1. Introduction

Plagioclase feldspars are among the most common minerals in the solar system and are regularly observed in meteorites such as the Shergottite–Nakhlite–Chassignite and the Howardite–Eucrite–Diogenite (HED) achondrite clans (Bridges & Warren 2006; Mittlefehldt 2015). Even ordinary chondrites, the most widespread clan originating from the S-type main belt asteroids, have plagioclases, besides olivine and pyroxenes, as the main mineral phases.

Nevertheless, in remote observations of asteroids, spectral features of plagioclases have never been unambiguously and directly observed. There is a strong consensus that Vesta, recently investigated in detail from a close orbit for about one year by the NASA *Dawn* mission (Russell et al. 2012), could be the parent body of the HED meteorite clan (McSween et al. 2011; Russell et al. 2012). Evidence that Vesta's terrains are consistent with HED mineralogy is based on Dawn's observations of the position of the two Fe^{2+} electronic transition bands of pyroxenes, located near 1 and 2 μm (De Sanctis et al. 2013). They have been used to map the distribution of these minerals on the Vesta surface (Ammannito et al. 2013a) because the wavelength positions of the band centers of HED lithologies vary between the meteorite groups, increasing in wavelength from Mg-rich pyroxenes (orthopyroxenitic diogenites), to Fe- and Ca-rich pyroxenes (basaltic eucrite), passing through howardites (Beck et al. 2017; which are brecciated mixtures of diogenites and eucrites).

Beside pyroxenes, the other main mineral phases composing the HEDs and expected to be found on their parent body, are the plagioclase feldspars, whose abundance is as high as 60% in cumulate eucrites, decreases in howardites, and is negligible in diogenites (Mittlefehldt 2015). In eucrites they are calcic, spanning the range An75-96 (Mittlefehldt 2015).

However, plagioclases have so far remained undetected by remote observations of Vesta, as spectral observations have been mostly performed in the visible to near-IR range where their spectra are nearly featureless. There are two exceptions: the very weak overtones and combination tones located between 4.6 and 6.2 μm (Nash & Salisbury 1991) and the weak crystal field absorption of Fe^{2+} at 1.25 μm that is observed only in plagioclases containing FeO impurities (Serventi et al. 2013). The spectral range around 10 μm, where fundamental molecular vibrations of Si/Al–O are located, is more diagnostic for plagioclases and for all silicate minerals (Salisbury 1993). The number and wavelength position of these bands can be used to detect the presence of different silicates and constrain their compositions. These absorptions produce typical spectral features such as the Reststrahlen bands (RBs) and the transparency feature (TF) in absorption, and the Christiansen feature (CF) in emission. They are also sensitive to granulometry, i.e., when decreasing grain size, TF, and CF are more prominent, whereas RB tends to disappear (Figure 1). Only a few Vesta observations have been performed in the mid-infrared range, conducted from the Kuiper Airborne Observatory (KAO) in 1992 (Cohen et al. 1998), from the *Infrared Space Observatory* (*ISO*) in 1997 (Dotto et al. 2000), and from the Palomar Observatory in 2001 (Lim et al. 2005).
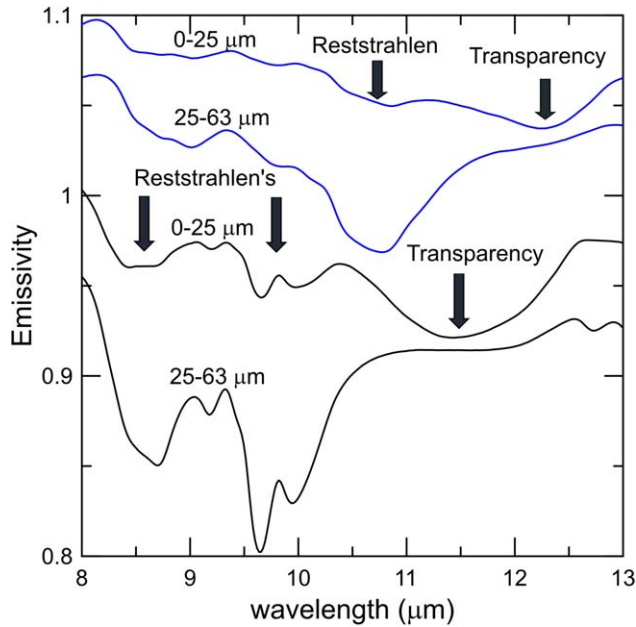
Figure 1. Emissivity spectra of the plagioclase feldspar end members at different grain sizes: anorthite 0–25 μm (blue), anorthite 25–63 μm (blue), albite 0–25 μm (black), and albite 25–63 μm (black). Reststrahlen features are stronger with increasing grain size, in contrast to transparency features, which disappear. Spectra are taken from the Berlin Emissivity Database (Maturilli 2015).

2. Observations and Results

2.1. New Telescopic Observations of Vesta

We performed new observations of Vesta in the mid-IR spectral range (8–13 μm) with the COMICS instrument at the 8.2 m Subaru Telescope at Mauna Kea, Hawaii. Observations were conducted in two campaigns in 2016 and 2017, obtaining a total of four full-disk spectra acquired during four different good-seeing nights (Figure 2). The observation's footprints cover most of the Vesta surface, allowing hemispherical discrimination in both longitude and latitude (Figure 3). This enables us to investigate the hemispherical asymmetry evidenced by the *Dawn* mission in pyroxene composition, with the mid-Northern latitudes being more eucritic-rich (Beck et al. 2017) and including the olivine deposits detected in the very northern regions (Ammannito et al. 2013b) and the multiple olivine enrichments suggested by spectral analyses at latitudes larger than 28° (Nathues et al. 2015; Palomba et al. 2015). From each observation, we obtained an absolute spectral flux and retrieved an absolute emissivity spectrum (see Appendices A and B).

All the spectra show a low spectral contrast but clear common spectral features (Figure 4). The most important spectrum is an absorption feature centered at 12.2–12.3 μm, ascribed to a plagioclase. This band is clearly detected, with a depth of 2%–3%, at the 2σ–3σ level in 2017 spectra and at the 1σ–2σ level in 2016. The interpretation of this feature is based on the comparison with emissivity laboratory spectra of plagioclase and pyroxene minerals available in spectral libraries (Maturilli et al. 2008) and also supported by new laboratory emissivity spectra of one eucrite and two howardites that we acquired at different grain sizes (see Appendix C in detail). The 12.2 μm feature, due to the higher transparency between the stretching and bending vibrational bands (Salisbury & Walter 1989), is present in emissivity spectra of fine plagioclase feldspars, with a center
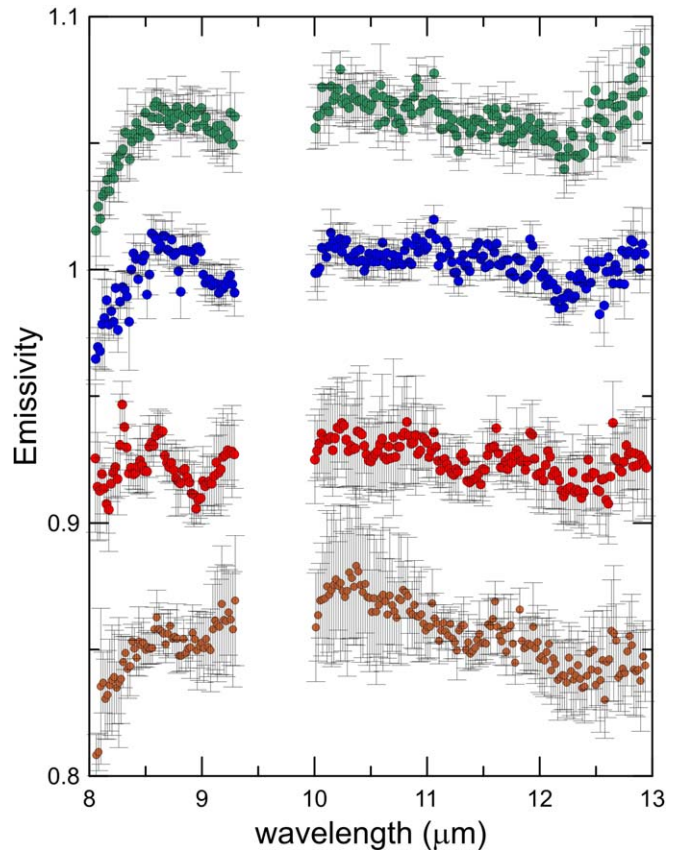

Figure 2. Vesta emissivity spectra taken from Subaru. The retrieved emissivity spectra were obtained on four different nights, shown from top to bottom: 2017 January 13, 12; 2016 January 24, 23. The 2017 spectral emissivity have a higher signal-to-noise ratio (S/N). Data between 9.3 and 10 μm are removed for telluric disturbance.

(The data used to create this figure are available.)

shifting shortward with increasing calcium content, toward the anorthite end member (Figure 5). This feature is observed when a plagioclase is crystalline and vanishes for shocked samples (Johnson et al. 2002). At increasing grain size, the strength of the TF decreases, contrary to RB, which deepens (Figure 1). Another feature observed in almost all the spectra is the principal CF, detected as a local maximum at 8.52 μm and compatible with pyroxene minerals. Weaker absorption features are present in some of the spectra and seem to be residual RBs, such as the one located at 11.2–11.4 μm. This feature is clearly present in the 2017 spectra above the 1σ level and it is at the detection limit in 2016 spectra due to the lower S/N. Its band center is compatible with a feature found in orthopyroxenes with large grain sizes (Hamilton 2000). No indications of olivine features are found. However, there are subtle but clear differences between the two campaigns, such as the presence of a weak band at 8.95 μm, possibly ascribed to pyroxenes, and a weakening of the 12.2 μm band in the 2016 spectra.

From the comparison of the measured band centers, we can infer that the Subaru TF is compatible with a crystalline calcium-rich plagioclase (Table 1). The strength of the TF is largely influenced by the grain size and is therefore very effective in constraining the global average grain size of the Vesta regolith. Laboratory spectra demonstrate that Ca-plagioclases show a well-developed TF only in the finest grain size fraction (0–25 μm), whereas TF disappears completely for
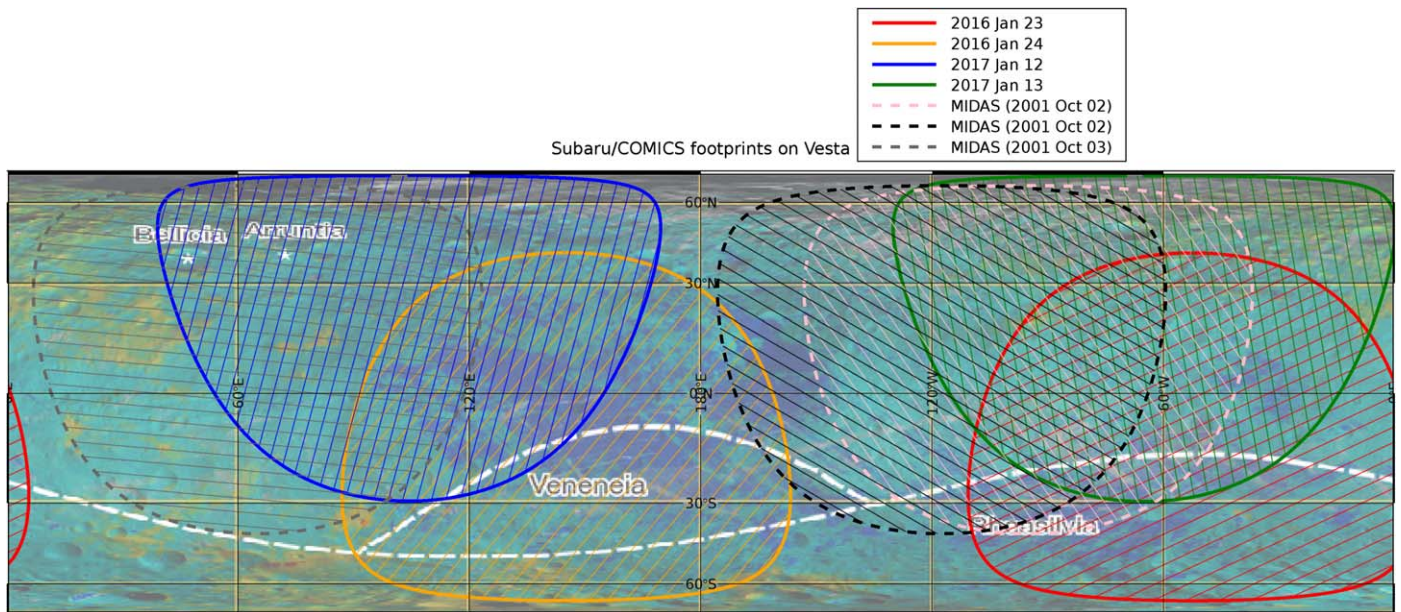
Figure 3. Footprints of the telescopic spectra. The four observations obtained at Subaru in 2016 and 2017, along with those of Palomar (MIDAS) observations, are shown; almost the entire Vesta surface is covered. The footprints are superimposed on the Vesta lithological map (Ammannito et al. 2013a) in which the eucritic regions are blue and the diogenitic ones are yellow.

the adjacent size interval (25–63 μm; Figure 1), indicating that on Vesta the global average grain size of plagioclases must be lower than a few tens of microns. A residual RB located at 11.4 μm, similar to that observed in Vesta's spectra, is present in the intermediate grain-sized eucrite sample (25–63 μm; Figure 4). Hence, spectral behavior pertaining to different grain sizes (at least for sizes lower than 63 μm) coexist in Subaru spectra. Independent thermal analyses obtained by ground-based and *Dawn* data indirectly also suggest a fine grain-sized regolith (Gundlach & Blum 2013; Capria et al. 2014). In particular, analysis of *Dawn*/VIR near-infrared spectra of Vesta, coupled with HED laboratory measurements, suggested a regolith grain size between 0 and 45 μm (Palomba et al. 2014). These evaluations are mostly pertaining to the physical properties of pyroxenes, whose contribution to the near-infrared spectral region is dominant. The Subaru-derived value provides information on the plagioclase grain size. The band depth of the TF at 12.2 μm gives an indication of the plagioclase abundance. A slight difference between the two hemispheres can be observed, with a band depth 15% shallower in the southern hemisphere. This result agrees with that obtained by *Dawn* (Beck et al. 2017), as a smaller abundance of plagioclases is expected in the diogenite-richer southern areas (Table 1).

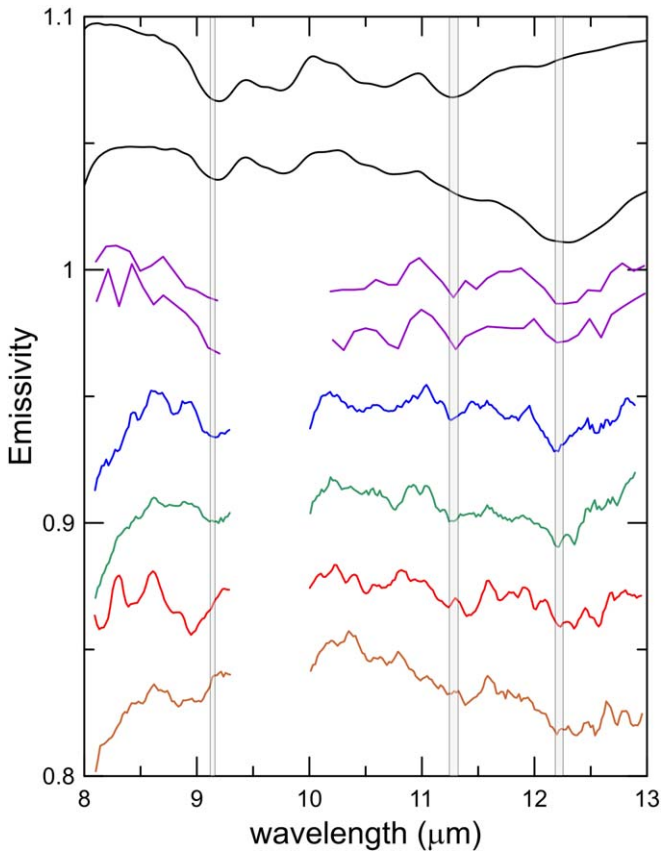### 2.2. Comparison with Previous Observations

To corroborate these findings, we have also re-examined mid-IR literature spectra of Vesta, taken by *ISO* and Palomar, discarding the KAO observations whose reliability is poor (M. Cohen 2019, personal communication). The *ISO* retrieved emissivity shows an anomalous large spectral contrast in emissivity and a questionable CF, located at wavelengths compatible with olivine that has been shown by more recent observations to be a minor component of the Vesta surface (Ammannito et al. 2013b; Palomba et al. 2015). The Palomar spectra cover mostly the northern hemisphere and show a very

low emissivity spectral contrast, very similar to our spectra 2017a and b. They also show both the TF at 12.2 μm and the band at 11.4 μm (Figure 4), features considered reliable but not discussed by the authors (Lim et al. 2005). The depths of these spectral features calculated on Subaru and Palomar spectra are comparable and are slightly larger than the fine howardites. At the same time, they are shallower than the pure anorthite, as expected in a regolith that is a mixture of plagioclase and pyroxenes (Table 1).

3. Discussion

#### 3.1. Ambiguity of the Unique Plagioclase Detection on Asteroid 1459 Magnya

We claim that our detection is the first ever made on asteroids. The only other detection of plagioclase on asteroids made so far is from a ground-based observation of the asteroid 1459 Magnya (Hardersen et al. 2004). It was claimed that plagioclases are abundantly present on the surface, with the spectra showing an inflection between 1 and 2 μm, centered at 1.17 μm and 10%, deep corresponding to a 37% of plagioclase abundance. However, this claim is not unambiguous. The band at 1.25, as it is called in this and other papers, is not native to plagioclase and appears only if iron is present on the plagioclase structure, with Fe^{2+} substituting for Ca^{2+} in sevenfold coordinated sites, causing the crystal field absorption (Burns 1993). This is the case, e.g., of lunar soils in which plagioclase contains significant amounts of iron (Bell & Mao 1973). However, even if iron is not present in large amounts in plagioclases, as is the case for the HED meteorites, the band can be still detected (Pieters et al. 2005). This is because the band is produced by the presence of Fe^{2+} in the M1 crystallographic site of pyroxenes (Burns 1993; Klima et al. 2007) that are abundant on HEDs. The strength of the 1.2 μm band is directly related to the proportion of the Fe^{2+} in the M1 site rather than to the total iron content in the pyroxenes

Figure 4. Comparison of Vesta with laboratory spectra and previous observation spectra. The smoothed emissivity spectra of Vesta obtained by Subaru observations in the bottom of the image (blue and green, 2017 campaign; red and light brown, 2016 campaign) are compared with the ones observed by Palomar observatory (purple) and laboratory spectra of HED (black). The HED spectra are stretched for the eucrite NWA7854 with grain sizes 25–63 μm (top) and the howardite NWA2698 grain sizes of 0–25 μm (bottom). The most important spectral features common to Subaru and the Palomar spectra are highlighted by gray lines. The 12.3 μm feature is common to Subaru, Palomar, and fine-grained howardite and is the TF due to plagioclases. The 11.4 μm feature due to residual RBs in pyroxenes is present in the eucrite emissivity but is not observed in the 2016 Subaru data. The 9.1 μm feature common to howardite and eucrite seems to be present in the 2017 Subaru data. A possible other residual feature (8.9 μm) likely to be assigned to pyroxenes is observed only in the 2016 Subaru data. The data spectral range between 9.3 and 10.0 μm were not shown because of strong telluric disturbances.

(The data used to create this figure are available.)

(ferrosilite; Klima et al. 2008). There is an additional inconsistency with the wavelength position of the Magnya putative plagioclase feature. The Fe^{2+} band has been well characterized in laboratories in iron-rich plagioclases (Serventi et al. 2013) on a suite of three samples and it is located at wavelengths between 1.26 and 1.30 μm, much larger than the detected value of 1.17 μm. In conclusion, the only published detection of a plagioclase on an asteroid is not unambiguous. Later on, when they were perhaps more aware of the complexity of the analysis, the same authors of the Magnya paper observed four other asteroids (Hardersen et al. 2006) and they were much more cautious about the assignment of this band, stating that more detailed interpretations are hampered by the ambiguity of the mineral producing the weak ∼1.3 μm absorption.
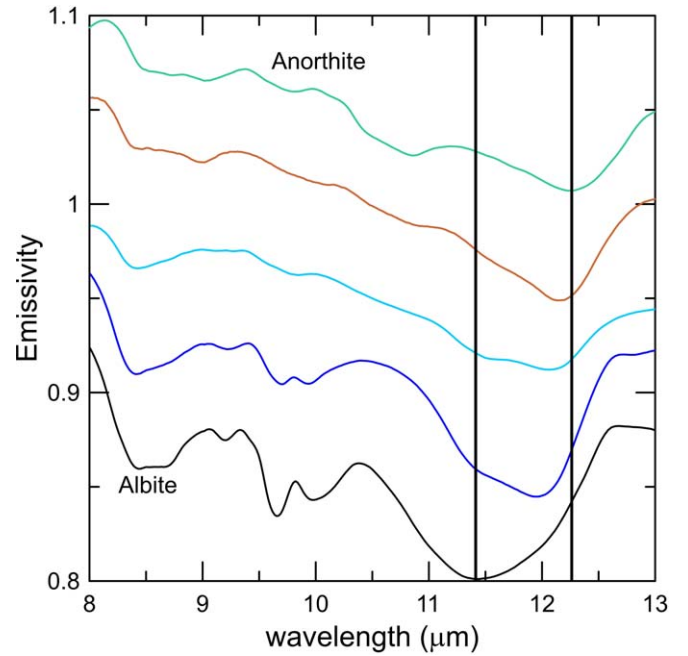
Figure 5. Emissivity spectra of the plagioclase series: anorthite (green), bytownite (orange), labradorite (light blue), andesine (blue), albite (black). The transparency feature shifts from 11.4 μm in albite to 12.3 μm in anorthite. Spectra are taken from the Berlin Emissivity Database (Maturilli 2015).

Table 1
Transparency Feature's Band Depth and Band Center

Spectrum	Band Depth (%)	Band Center (μm)
Subaru (2016a)	2.2	12.3
Subaru (2016b)	2.2	12.3
Subaru (2017b)	2.6	12.2
Subaru (2017c)	2.6	12.2
Palomar1	1.9	12.2
Palomar2	1.4	12.3
NWA6309	1.4	12.2
NWA2698	1.5	12.3
Anorthite	3.7	12.3
Bytownite	5.2	12.2
Labradorite	5.4	12.1
Andesine	3.2	12.1
Albite	3.8	11.5

Note. As measured in MIR telescopic spectral emissivities from Vesta's observational campaigns (Subaru and Palomar), in two howardites, NWA6309 and NWA2698, and in a series of plagioclases with decreasing calcium content from anorthite to albite. The BC shifts shortward as the calcium content decreases. The BD is 15% lower in the 2016 campaign during which Vesta's southern hemisphere was observed.

3.2. Nature of Plagioclases on Vesta

A plagioclase comprises a solid solution series ranging from calcium-rich anorthite ($CaAl_2Si_2O_8$) to sodium-rich albite ($NaAlSi_3O_8$), whose composition is typically expressed in terms of anorthite or albite content. For fine-grained plagioclases (0–25 μm) the transparency feature can be detected. This feature shifts to shorter wavelengths as the calcium content decreases (sodium increases). TF is strongly affected by shock pressure and its band depth decreases with increasing shock, eventually disappearing when all the plagioclase is transformed

to diaplectic glass for shock pressures larger than about 40 GPa (Johnson et al. 2002). This happens because the structural disorder in the shocked samples prevents significant volume scattering (Johnson et al. 2002). The transformation of plagioclase in diaplectic glass corresponds to shock class 2 (Kieffer et al. 1976). In the case of the Vesta regolith, there would be two kinds of impacts with different combinations of impactor/target: dense–porous (macrometeoroids versus fine regolith) and dense–dense (micrometeoroids versus fine regolith). Using the projectile velocity–pressure relation associated with the classes of shock (Hörz & Schaal 1981), we can predict the maximum velocity for impactors and micrometeorites at Vesta to preserve the crystalline habit of plagioclase. Class 2 is produced for impact velocities of 4–5.5 km s^{-1} and 3.6–5.1 km s^{-1} for a dense–porous and dense–dense case, respectively. The estimated average velocity of impactors at Vesta is 5 km s^{-1}, slightly larger than the primordial velocity (4.7 km s^{-1}) before the late heavy bombardment (Marchi et al. 2013), but it can be even larger for a micrometeoroid whose largest part is provided by the Jupiter comet family fragmentation. Because plagioclases found on Vesta are clearly crystalline, they cannot be produced solely by impacts and a milder process such as the thermal fatigue should be invoked. This process is a crucial mechanism in the production of regolith in near-Earth Asteroids, where boulders present on the surface experiences cyclic diurnal temperature variations, which cause mechanical stresses with the formation of cracks and their propagation throughout the rocks (Delbo et al. 2014). Finally, rocks break down and contribute to the generation of regolith and this would be very effective to regolith grain size down to millimeters. In order to produce such a fine and crystalline regolith on Vesta, a well-combined balance between impacts and thermal fragmentation should be active: by breaking down rocks into smaller pieces and thus exposing new surface area, thermal fragmentation can provide a mechanism to make fresh regolith, becoming a crucial mechanism of surface rejuvenation where fresh, unshocked plagioclase grains can somehow be constantly resupplied to the surface regolith.

4. Conclusions

Detection of a spectroscopic feature of abundant Ca-rich plagioclase feldspars on Vesta provides additional strong, if not definitive, evidence that Vesta is the parent body of the HED meteorites. The fact that this feature is slightly stronger in the northern regions is in agreement with the distribution of eucritic and howarditic materials found by *Dawn* (Beck et al. 2017). The retrieved fine grain size of plagioclases, very close to those obtained for pyroxene, reflects the high efficiency of the mechanical brecciation that produced a quasi-homogenization in size of both the main mineral phases present on Vesta. It is recognized, indeed, that Vesta experienced a particular type of space weathering in which the role of the solar wind and micrometeoritic interactions is largely reduced in favor of regolith mobilization and fine-scale mixing (Pieters et al. 2012). However, this scenario does not give the process of brecciation the importance it deserves in forming the regolith grains. We argue for thermal fatigue (Delbo et al. 2014) to be an important process in the Vesta regolith formation. In fact, it should be at least as efficient as the concomitant micrometeoroid impacts, since fragmentation with large shock pressure transferred by the impacts would have transformed a large

portion of plagioclases into diaplectic glass (maskelynite), making their detection impossible through the transparency feature. Thus, thermal fragmentation should be considered one of the most important processes governing regolith production and regeneration not only on coarse-grained regolith present on small asteroids near the Earth (Delbo et al. 2014), but even on fine-grained regoliths of larger asteroids in the main belt, where thermal gradients are much lower.

Appendix A
Data Reduction

We carried out the N-band (8–13 μm) low-resolution spectroscopy ($R \sim 250$) of Vesta with the Cooled Mid-Infrared Camera and Spectrometer (COMICS; Kataza et al. 2000) mounted on the 8.2 m Subaru Telescope in Mauna Kea, USA, on two occasions: 2016 January 23–24 (Subaru normal program: S15B-049) and 2017 January 12–14 (S16B-021) in UTC. In the case of COMICS spectroscopy, all the photons from object do not fall onto the slit (i.e., the slit width of 0″33 is narrower than a typical seeing size) and the ratio of the loss to the total flux depends on wavelength. Therefore, in order to correct the loss (referred to as slit efficiency) and then derive the absolute spectrum, we also took Vesta images at 8.73 and 12.44 μm. HD5112 (spectral type: M0III) and HD62721 (K5III) were selected as the standard star for 2016 and 2017 observations, respectively.

The observation methodology and data reduction are explained in detail by Sato et al. (2014) and here we repeat the basic relations. The absolute disk-integrated flux of Vesta $\overline{\pi F_v}$ at a wavelength λ_i was computed with

$$\overline{\pi F_v}(\lambda_i) = \frac{\int \pi F_v(\lambda) \cdot \frac{\lambda}{hc} \cdot \phi(\lambda) d\lambda}{\int \frac{\lambda}{hc} \cdot \phi(\lambda) d\lambda} = \frac{\sum_j C_V(\lambda_i, j)}{\sum_j C_S(\lambda_i, j)}$$
$$\cdot \frac{a_V \lambda_i + b_V}{a_S \lambda_i + b_S} \cdot \frac{\int \pi F_S(\lambda) \cdot \frac{\lambda}{hc} \cdot \phi(\lambda) d\lambda}{\int \frac{\lambda}{hc} \cdot \phi(\lambda) d\lambda}, \qquad (1)$$

where $\pi F_v(\lambda)$ is the Vesta flux at wavelength λ, h is Planck's constant, c is the velocity of light, $\phi(\lambda)$ is the instrument-response function consisting of the COMICS optics, the N-band broad bandpass filter, the grating, and the array detector, i and j are indices for wavelength and slit length directions, respectively, $\sum_j C_V(\lambda_i, j)$ and $\sum_j C_S(\lambda_i, j)$ are the spatially integrated count rates of Vesta and standard star at the wavelength λ_i, respectively, a_V and b_V (a_S and b_S) are the coefficients of slit efficiency for Vesta (standard star), and $\pi F_s(\lambda)$ is the flux of standard star as a function of wavelength

λ. The term λ/hc is added to represent the energy in units of numbers of photons. The slit efficiency, which can be represented by a linear function, was determined so that the values at 8.73 and 12.44 μm derived by convolving the spectrum with their filter transmission curves are equal to the disk-integrated flux obtained from imaging data.

Appendix B
Retrieval of Spectral Emissivity and Band Depth

We derived a spectral emissivity independently from each observation. This is achieved by inverting a model of the full-disk spectral flux fitted to the observation, with a total of four free parameters. Although COMICS observations do not resolve the Vesta's disk, the full-disk flux depends primarily on the distribution of emission angles and temperatures over the observed hemisphere, which in turn depends on the distribution of incidence angles. Hence, we reconstructed the appearance of Vesta for each observing time by taking advantage of JPL's SPICE NAIF tools (Acton 1996) and a shape model for Vesta topography provided by the *Dawn* mission. Hence, the Vesta apparent disk is subdivided into a number of surface elements small enough to be characterized by a single value of emission angle (e_{xy}) and incidence angle (i_{xy}). The latter is used to assign to the surface element a temperature value $T_{xy} = T_{SS} f(i_{xy})$, where T_{SS} represents the sub-solar temperature and $f(i)$ is a polynomial function inferred from the Dawn surface temperature analysis (Tosi et al. 2014). The total flux is then obtained by integrating the fluxes of single surface elements over the solid angles ($d\omega_{xy}$) they subtend to the observer, neglecting the contribution of spatial variations of albedo and roughness:

$$F_m(\lambda) = \frac{a\,\bar{\epsilon}}{1 + \eta\bar{\epsilon}} \int_{\Omega} B[\lambda; T_{xy}] \cos(e_{xy}) d\omega_{xy}. \tag{2}$$

Here $\bar{\epsilon}$ represents a disk- and spectral-averaged surface emissivity; η is a disk-averaged surface roughness; Ω is the total solid angle subtended by the Vesta's disk; $B(\lambda, T_{xy})$ is the Planckian emission at wavelength λ of a Vesta surface element. The factor $1/(1 + \eta\bar{\epsilon})$ is the adopted representation of the beaming factor, useful to account for the scattering contribution due to surface roughness. The a parameter is a scaling factor for balancing small biases introduced by calibration and model assumptions.

Finally, equation (2) is used to invert the observation by keeping $\bar{\epsilon}$, a, η, T_{SS} as free parameters. Hence, the final spectral emissivity is obtained from the best-fitting model as $\epsilon(\lambda) = \bar{\epsilon} F_{obs}(\lambda)/F_{m,best}(\lambda)$.

The procedure of retrieval of TF band strength was the same for Vesta and laboratory emissivity spectra. We considered the local minimum in the range 11.5–12.8 μm and the closer longward and shortward local maxima. The spectral continuum is the straight line between the two local maxima. The band strength is given by $1 - \varepsilon_m/\varepsilon_{cont}$, where ε_m and ε_{cont} are the emissivity and the continuum at local minimum, respectively.

Appendix C
Meteorite Samples and Experimental Setup

For the interpretation of the Subaru data, emissivity spectra of three powder samples of HED meteorites were newly acquired at the PEL Planetary Emissivity Laboratory (PEL)/ PSL (Planetary Spectroscopy Laboratory), at DLR, Berlin. The setup consists of an external emissivity chamber (DLR custom design) attached to a Bruker Vertex80V FTIR from the visible to the mid-IR (from 1 to 16 μm; Maturilli et al. 2008). An additional heating system controlled by an external power supply was used to heat up the stainless steel cups that contained the samples, were able to work from 293 to 343 K, and maintained under purged air during the measurement acquisition. The sample holder (50 mm in diameter and from 1 to 3 mm in thickness) requires from 3 to 5 grams of sample. The incident angle range was between 30° and 50°, while the working temperature (monitored by a thermocouple in thermal contact with the cup) was 373 K. The packed powder samples were prepared by means of a sieve system able to prepare different intervals of grain sizes of 0–25 and 25–63 μm. The calibration was made by means of a blackbody controlled at 303 K.

The meteorites used for the emissivity analysis are as follows:

1. NWA2698 (howardite); geochemistry: eucritic pyroxene: $Fs_{47.2-0}$ Wo_{7-18}, shock degree 3–5 (*The Meteoritical Bulletin*, No. 90, 2006, 1282-1416).
2. NWA6309 (polymict eucrite); geochemistry: low-Ca pyroxene $Fs_{56.7-57.4}$, $Wo_{5.9-6.3}$; Ca-pyroxene $Fs_{28-35.4}$ $Wo_{32.7-42.1}$; calcic plagioclase $An_{90.1-91.8}$ (*The Meteoritical Bulletin*, No. 102, 2015, 1662).
3. NWA7854 (polymict eucrite); geochemistry: low-Ca px $Fs_{35.5-47.9}$ $Wo_{1.3-4}$; FeO/MnO = 28-32; Ca-pyroxene $Fs_{18-32.2}$ $Wo_{24-44.7}$; FeO/MnO = 25-31; calcic plagioclase: $An_{85.3-92.2}$ (*The Meteoritical Bulletin,* No. 102, 2015, 1662).

The powder samples of NWA2698 (0–25 μm), NWA6309 (0–25 μm), and NWA7854 (0–25 and 25–63 μm) were analyzed by heating each sample at 370 K.

ORCID iDs

E. Palomba ⓘ https://orcid.org/0000-0002-9101-6774
E. D'Aversa ⓘ https://orcid.org/0000-0002-5842-5867
F. Oliva ⓘ https://orcid.org/0000-0002-6271-3722

References

Acton, C. H. 1996, P&SS, 44, 65
Ammannito, E., De Sanctis, M. C., Capaccioni, F., et al. 2013a, M&PS, 48, 2185
Ammannito, E., De Sanctis, M. C., Palomba, E., et al. 2013b, Natur, 504, 122
Beck, A. W., Lawrence, D. J., Peplowski, P. N., et al. 2017, Icar, 286, 35
Bell, P. M., & Mao, H. K. 1973, Year Book-Carnegie Institution of Washington, Vol. 72 (Washington, DC: Carnegie Institution of Washington), 574
Bridges, J. C., & Warren, P. H. 2006, JGSoc, 163, 229
Burns, R. G. 1993, Mineralogical Applications of Crystal Field Theory, Vol. 5 (Cambridge: Cambridge Univ. Press)
Capria, M. T., Tosi, F., De Sanctis, M. C., et al. 2014, GeoRL, 41, 1438
Cohen, M., Witteborn, F. C., Roush, T., Bregman, J., & Wooden, D. 1998, AJ, 115, 1671
De Sanctis, M. C., Ammannito, E., Capria, M. T., et al. 2013, M&PS, 48, 2166
Delbo, M., Libourel, G., Wilkerson, J., et al. 2014, Natur, 508, 233
Dotto, E., Müller, T. G., Barucci, M. A., et al. 2000, A&A, 358, 1133
Gundlach, B., & Blum, J. 2013, Icar, 223, 479
Hamilton, V. E. 2000, JGRE, 105, 9701
Hardersen, P. S., Gaffey, M. J., & Abell, P. A. 2004, Icar, 167, 170
Hardersen, P. S., Gaffey, M. J., Cloutis, E. A., Abell, P. A., & Reddy, V. 2006, Icar, 181, 94
Hörz, F., & Schaal, R. B. 1981, Icar, 46, 337

Johnson, J. R., Hörz, F., Lucey, P. G., & Christensen, P. R. 2002, JGRE, 107, 5073

Kataza, H., Okamato, Y., Takubo, S., et al. 2000, Proc. SPIE, 4008, 1144

Kieffer, S. W., Schaal, R. B., Gibbons, R., et al. 1976, LPSC, 7, 1391

Klima, R. L., Pieters, C. M., & Dyar, M. D. 2007, M&PS, 42, 235

Klima, R. L., Pieters, C. M., & Dyar, M. D. 2008, M&PS, 43, 1591

Lim, L. F., McConnochie, T. H., Bell, J. F., & Hayward, T. L. 2005, Icar, 173, 385

Marchi, S., Bottke, W. F., Cohen, B. A., et al. 2013, NatGe, 6, 303

Maturilli, A. 2015, BED Emissivity Spectral Library, figshare, version 1, doi:10.6084/m9.figshare.1536469.v1

Maturilli, A., Helbert, J., Moroz, L., et al. 2008, P&SS, 56, 420

McSween, H. Y., Mittlefehldt, D. W., Beck, A. W., Mayne, R. G., & McCoy, T. J. 2011, SSRv, 163, 141

Mittlefehldt, D. W. 2015, ChEG, 75, 155

Nash, D. B., & Salisbury, J. W. 1991, GeoRL, 18, 1151

Nathues, A., Hoffmann, M., Schäfer, M., et al. 2015, Icar, 258, 467

Palomba, E., Longobardo, A., De Sanctis, M. C., et al. 2014, Icar, 240, 58

Palomba, E., Longobarto, A., De Sanctis, M. C., et al. 2015, Icar, 258, 120

Pieters, C. M., Binzel, R. P., Bogard, D., et al. 2005, in IAU Symp. 229, Asteroids, Comets, Meteors, ed. D. Lazzaro (Cambridge: Cambridge Univ. Press), 273

Pieters, C. M., Ammannito, E., Blewitt, D. T., et al. 2012, Natur, 491, 79

Russell, C. T., Raymond, C. A., Coradini, A., et al. 2012, Sci, 336, 684

Salisbury, J. W. 1993, in Remote Geochemical Analysis: Elemental and Mineralogical Composition, ed. C. M. Pieters & P. A. J. Englert (Cambridge: Cambridge Univ. Press), 79

Salisbury, J. W., & Walter, L. S. 1989, JGRB, 94, 9192

Sato, T. M., Sagawa, H., Kouyama, T., et al. 2014, Icar, 243, 386

Serventi, G., Carli, C., Sgavetti, M., et al. 2013, Icar, 226, 282

Tosi, F., Capria, M. T., De Sanctis, M. C., et al. 2014, Icar, 240, 36